

## Improving the accuracy of mass-lumped finite-elements in the first-order formulation of the wave equation by defect correction

Shamasundara, R.; Mulder, Wim

**DOI**

[10.1016/j.jcp.2016.07.006](https://doi.org/10.1016/j.jcp.2016.07.006)

**Publication date**

2016

**Document Version**

Accepted author manuscript

**Published in**

Journal of Computational Physics

**Citation (APA)**

Shamasundara, R., & Mulder, W. (2016). Improving the accuracy of mass-lumped finite-elements in the first-order formulation of the wave equation by defect correction. *Journal of Computational Physics*, 322, 689-707. <https://doi.org/10.1016/j.jcp.2016.07.006>

**Important note**

To cite this publication, please use the final published version (if applicable). Please check the document version above.

**Copyright**

Other than for strictly personal use, it is not permitted to download, forward or distribute the text or part of it, without the consent of the author(s) and/or copyright holder(s), unless the work is under an open content license such as Creative Commons.

**Takedown policy**

Please contact us and provide details if you believe this document breaches copyrights. We will remove access to the work immediately and investigate your claim.

# Improving the accuracy of mass-lumped finite-elements in the first-order formulation of the wave equation by defect correction

R. Shamasundar<sup>a,1</sup>, W.A. Mulder<sup>a,b</sup>

<sup>a</sup>*Delft University of Technology, Faculty of Civil Engineering and Geosciences, Department of Geoscience & Engineering, P.O.Box 5048, 2600 GA Delft, Netherlands*

<sup>b</sup>*Shell Global Solutions International, Kessler Park 1, 2288 GS Rijswijk, The Netherlands*

---

## Abstract

Finite-element discretizations of the acoustic wave equation in the time domain often employ mass lumping to avoid the cost of inverting a large sparse mass matrix. For the second-order formulation of the wave equation, mass lumping on Legendre-Gauss-Lobatto points does not harm the accuracy. Here, we consider a first-order formulation of the wave equation. In that case, the numerical dispersion for odd-degree polynomials exhibits super-convergence with a consistent mass matrix and mass lumping destroys that property. We consider defect correction as a means to restore the accuracy, in which the consistent mass matrix is approximately inverted using the lumped one as preconditioner. For the lowest-degree element, fourth-order accuracy in 1D can be obtained with just a single iteration of defect correction.

The numerical dispersion curve describes the error in the eigenvalues of the discrete set of equations. However, the error in the eigenvectors also play a role, in two ways. For polynomial degrees above one and when considering a 1-D mesh with constant element size and constant material properties, a number of modes, equal to the maximum polynomial degree, are coupled. One of these is the correct physical mode that should approximate the true eigenfunction of the operator, the other are spurious and show have a small amplitude when the true eigenfunction is projected onto them. We analyse the behaviour of this error as a function of the normalized wavenumber in the form of the leading terms in its series expansion and find that this error exceeds the dispersion error, except for the lowest degree where the eigenvector error is zero. Numerical 1-D tests confirm this behaviour.

We briefly analyze the 2-D case, where the lowest-degree polynomial also appears to provide fourth-order accuracy with defect correction, if the grid of squares or triangles is highly regular and material properties constant.

*Keywords:* Finite Element Method, Mass Lumping, Wave Equation

---

## 1. Introduction

Numerical simulation of the wave equation in the time domain can be accomplished by a suitable finite-difference method. This method is relatively easy to implement and parallelize. High-order differencing is often used to improve both computational and memory efficiency. For problems with sharp velocity contrasts, however, the finite-difference method is less attractive, because the solution is not sufficiently smooth across these contrasts and sharp interfaces between different materials cannot be easily represented on a finite-difference grid. In numerical simulations of wave propagation, this produces stair-casing, as shown in Fig. 1 of [1]. This may be a serious drawback for seismic applications in complex geologies [2].

The finite-element method can, in principle, overcome these difficulties if element faces follow sharp contrasts. Mass lumping is usually applied to avoid the cost of inverting a large sparse consistent mass matrix. However, mass lumping may cause a loss of spatial accuracy. This is not true for the second-order formulation of the wave equation. The choice of Legendre polynomials and Gauss-Lobatto points actually leads to better accuracy after mass lumping, as proven in the Appendix of [3]. These results were confirmed later by [4, 5].

---

*Email address:* R.Shamasundar@tudelft.nl (R. Shamasundar)

For variable-density acoustics as well as the elastic system of wave equations, a first-order formulation can sometimes be more convenient. In the 1-D acoustic case, this provides a pair of equations in the pressure and in the particle velocity. The usual finite-element discretization involves different spaces for each, for instance,  $H^1$  and  $L^2$ . If the solution is represented by polynomials with and without continuity across elements, the first-order formulation can be made identical to the second-order one [6, section 13.4.2]. Here, we adopt the naive approach of discretizing each of the pair of first-order equations for pressure and velocity with the same spectral-element method.

Unfortunately, the application of mass lumping to first-order differentiation with Legendre-Gauss-Lobatto (LGL) points leads to a decrease of accuracy [7]. In this paper, we propose to use defect correction [8] to compensate for this loss of accuracy. Defect correction employs a lower-order discretization of a problem as a preconditioner for a higher-order discretization. The gain in accuracy per iteration is the same as that of the lower order [8, section 7]. If, for instance, an operator with fourth-order accuracy is preconditioned by one with second-order accuracy, the first step provides an approximate solution with second-order accuracy. One additional iteration already leads to fourth-order accuracy if the numerical solution is sufficiently well resolved by the discretization to lie in the asymptotic regime where it converges.

In the work of [9], the diagonal of the mass matrix was used as a pre-conditioner to the consistent mass matrix. Here, we will show that method to be less effective.

To investigate the properties of the proposed scheme, we perform the same type of dispersion analysis as in [3], but now on a discrete operator that represents the first instead of the second derivative in space. If the polynomial basis has degree  $M$ , a discrete Fourier transform of the discrete operator results in a matrix with small  $M \times M$  blocks, for which eigenvalues and eigenvectors can be determined, numerically or symbolically or as a series approximation for small wavenumbers. Each of the  $M$  eigenmodes deals with one separate point on the dispersion curve. Their interaction can be characterized as ‘spurious’ and was quantified in [3] by considering the eigenvector errors. An alternative approach was followed by [10, 4, 6], where the eigenvectors were constructed directly and then the eigenvalues that constitute the dispersion curve were determined.

We examined the numerical dispersion curves and error behaviour for four schemes with polynomial basis functions: the standard elements with equidistant nodes (EQUI), the Legendre-Gauss-Lobatto points (LGL), the Chebyshev-Gauss-Lobatto nodes without a weighting function [11] (CGL) and with (CGLw). Section 2 describes the various discretizations, how we apply defect correction and analyze the numerical dispersion. Section 3 lists the leading error terms in the dispersion curves for the consistent mass matrix, for the lumped one, and after one iteration of defect correction. It includes estimates of the error in the eigenvectors. Numerical experiments for simple differentiation as well as for 1-D wave propagation on a periodic mesh are included. In Section 4, we apply Fourier analysis on a periodic grid to obtain error estimates for the 2-D case, both for square bilinear elements and for squares cut onto half to obtain a regular mesh of triangles. Section 5 summarizes our findings.

## 2. Method

### 2.1. Elements

A first-order formulation of the acoustic wave equation is

$$\rho \frac{\partial v}{\partial t} = \frac{\partial p}{\partial x}, \quad \frac{1}{\rho c^2} \frac{\partial p}{\partial t} = \frac{\partial v}{\partial x},$$

with particle velocity  $v(t, x)$  and pressure  $p(x, t)$  (actually without the minus sign) as function of time  $t$  and position  $x$ . The density  $\rho(x)$  and sound speed  $c(x)$  will be taken as constant for the purpose of analysis. We will not consider time stepping errors and only concentrate on the spatial discretisation. Consider  $N$  elements bounded by positions  $x_j = x_0 + jh_j$ ,  $j = 0, \dots, N$ . Each element has  $M + 1$  nodes at relative positions  $\zeta_k$ ,  $k = 0, \dots, M$ , with  $\zeta_0 = -1$  and  $\zeta_M = 1$ . Their corresponding global positions are  $x_{j,k} = x_j + \frac{1}{2}(\zeta_k + 1)jh_j$ . In the periodic case, the solution on  $x_N$  is the same as on  $x_0$ . The number of degrees of freedom is  $N_{\text{dof}} = MN$  on a periodic grid both for the particle velocity and pressure.

For the finite-element basis functions  $\psi_k(\zeta)$ , we take the Lagrange interpolating polynomials of degree  $M$  relative to the nodes, so  $\psi_k(\zeta_l) = \delta_{k,l}$ , the Kronecker delta. In each element, we have a local mass matrix  $A$  and first-derivative

matrix  $D$ , each with entries

$$A_{k,l} = \int_{-1}^1 w(\zeta) \psi_k(\zeta) \psi_l(\zeta) d\zeta, \quad D_{k,l} = \int_{-1}^1 w(\zeta) \psi_k(\zeta) \frac{d}{d\zeta} \psi_l(\zeta) d\zeta.$$

The local lumped mass matrix,  $A_{k,l}^L = \delta_{k,l} \sum_{l=0}^M A_{k,l}$  is a diagonal matrix with values proportional to quadrature weights. We consider four choices for the nodes: the standard element with equidistant nodes  $x_k = k/M$ ,  $k = 0, 1, \dots, M$  (EQUI); the Legendre-Gauss-Lobatto points (LGL) that are the zeros of  $(1 - \zeta^2)P'_M(\zeta)$ , the Chebyshev-Gauss-Lobatto points  $\zeta_k = -\cos(\pi k/M)$  with an unweighted scalar product (CGL) and with the weighting function  $w(\zeta) = 1/\sqrt{1 - \zeta^2}$  (CGLw). Numerical quadrature with weights  $A_{k,k}^L / \sum_{k=0}^M A_{k,k}^L$  is exact for polynomials up to degree  $q = 1 + 2 \text{ floor}\{M/2\}$  for CGL and EQUI and degree  $q = 2M - 1$  for LGL and CGLw.

## 2.2. Mass matrix and defect correction

With the local mass and first-derivative matrices, we can assemble the global mass matrix  $\mathcal{M}$  and derivative matrix  $\mathcal{D}$ . A leap-frog time discretisation with time step  $\Delta t$  is

$$\frac{1}{\Delta t} \mathcal{M}_v(\mathbf{v}^{n+1} - \mathbf{v}^n) = \mathcal{D}_p \mathbf{p}^{n+1/2}, \quad \frac{1}{\Delta t} \mathcal{M}_p(\mathbf{p}^{n+3/2} - \mathbf{p}^{n+1/2}) = \mathcal{D}_v \mathbf{v}^{n+1}. \quad (1)$$

Here, the material properties are absorbed into the mass matrices and the superscript  $n$  denotes the solution at time  $t^n = t_0 + n\Delta t$ . Note that we have made a distinction between the first-derivative operators  $\mathcal{D}_p$  and  $\mathcal{D}_v$ , but for the periodic problems considered later on in the analysis and numerical tests, they will be taken the same. As shown in Appendix A, the time-stepping stability limit for a leap-frog scheme is given by the CFL number  $2\rho^{-1/2}(\overline{\mathcal{L}})$ , with  $\overline{\mathcal{L}} = -\mathcal{M}_p^{-1} \mathcal{D}_v \mathcal{M}_v^{-1} \mathcal{D}_p$  and where  $\rho(\cdot)$  now denotes the spectral radius. For time stepping, we want to avoid the cost of inverting the consistent mass matrix and replace it by its lumped version. Depending on the choice of nodes, this may or may not harm the spatial accuracy. Formally, the lumped version should be exact for numerical quadrature of polynomials up to a degree of at least  $2M - 2$  for the second-order form of the wave equation and  $2M - 1$  for the first-order form. If its accuracy is less, we can iterate with the lumped mass matrix as preconditioner. This approach resembles defect correction [8], which has the following convenient property. Consider two operators  $\mathcal{L}_1$  and  $\mathcal{L}_2$  where  $\mathcal{L}_k$  has an order of accuracy  $p_k$  ( $k = 1, 2$ ) and  $p_1 > p_2$ . We can try to solve  $\mathcal{L}_1 \mathbf{u} = \mathbf{f}$  with the iterative scheme  $\mathbf{u}^{-1} = 0$ ,  $\mathbf{u}^{j+1} = \mathbf{u}^j + \mathcal{L}_2^{-1}(\mathbf{f} - \mathcal{L}_1 \mathbf{u}^j)$ , where  $j = 0, 1, \dots$  denotes the iteration count, not the time step. Convergence is obtained if the operator  $\mathcal{G} = \mathcal{I} - \mathcal{L}_2^{-1} \mathcal{L}_1$  has a spectral radius  $\rho(\mathcal{G}) < 1$ . In a finite-difference context, the order of accuracy of  $\mathbf{u}^j$  is  $\min(p_2, (j+1)p_1)$ , which suggests that a few iterations will often suffice to get a sufficiently accurate though not necessarily fully converged result [8]. In our case, we can take the lumped mass matrix for  $\mathcal{L}_2 = \mathcal{M}^L$  and the consistent mass matrix as  $\mathcal{L}_1 = \mathcal{M}$ . However, for degree  $M > 1$ , the eigenvalues and eigenvectors are mixed up in a non-trivial way [3] and the property that the accuracy increases by an order  $p_1$  per iteration may be lost.

## 2.3. Dispersion

The numerical dispersion of the finite-element scheme can be analyzed by considering the eigenvalues of the first-order operator  $\mathcal{M}^{-1} \mathcal{D}$  or  $(\mathcal{M}^L)^{-1} \mathcal{D}$  when discretized on a sufficiently fine periodic mesh with constant material properties and a constant element size  $h$ . Alternatively, we can use the fact that the elements are translation-invariant if all is constant and perform a Fourier transform on the solution. We then have to take the  $M$  degrees of freedom inside an element as a vector and do a transform on each component over the  $N$  elements. This results in a small  $M \times M$  matrix in the Fourier domain. However, we can go one step further and also involve the  $M$  individual components. These are aliased but still can be considered separately by looking at the eigenvalues of the  $M \times M$  block and unwrapping the result [3]. This produces a discrete approximation  $i\kappa$  to the exact operator  $i\xi$ , where  $\xi = k(x_N - x_0)/(NM) = kh/M \in [-\pi, \pi]$  is scaled version of the wavenumber  $k$ . The relative dispersion error can then be characterized by  $\kappa/\xi - 1$ . Note that the error in the dispersion curve does not tell the full story, because errors in the eigenvectors also play a role.

Table 1: Leading error terms in the dispersion curves for a polynomial basis of degree  $M$  and various sets of nodes, using the consistent or lumped mass matrix or lumped with one iteration based on  $\mathcal{G}$ . Its spectral radius  $\rho(\mathcal{G})$  is given, as well as the CFL number without and with mass lumping.

$M$	nodes	consistent	lumped	1 iteration	$\rho(\mathcal{G})$	CFL (consist.)	CFL (lumped)	CFL (1 iter.)
1	LGL	$-\frac{1}{180}\xi^4$	$-\frac{1}{6}\xi^2$	$-\frac{1}{30}\xi^4$	2/3	$2/\sqrt{3} = 1.155$	2	1.457
2	LGL	$\frac{1}{270}\xi^4$	$-\frac{4}{270}\xi^4$	$-\frac{4}{945}\xi^4$	3/5	$\sqrt{2}/3 = 0.471$	$2/3 = 0.667$	0.535
3	LGL	$-\frac{81}{39200}\xi^8$	$-\frac{27}{2800}\xi^6$	$-\frac{3}{1400}\xi^6$	4/7	0.278	0.365	0.308
4	LGL	$\frac{128}{496125}\xi^8$	$-\frac{1024}{496125}\xi^8$	$-\frac{4096}{6449625}\xi^8$	5/9	0.188	0.239	0.208
5	LGL	$\frac{-9765625}{19179224064}\xi^{12}$	$\frac{-78125}{67060224}\xi^{10}$	$\frac{-15625}{50295168}\xi^{10}$	6/11	0.138	0.171	0.151
3	CGL	see LGL	$-\frac{333}{10240}\xi^4$	$-\frac{21}{1460}\xi^2$	3/5	see LGL	0.311	0.342
4	CGL	see LGL	$\frac{8}{1395}\xi^4$	$-\frac{1042}{35397}\xi^4$	5/7	see LGL	0.198	0.247
5	CGL	see LGL	$-\frac{231125}{134217728}\xi^4$	$\frac{5115}{4502764}\xi^2$	0.966	see LGL	0.132	0.203
1	CGLw	$-\frac{1}{24}\xi^2$	$-\frac{1}{6}\xi^2$	$-\frac{1}{24}\xi^2$	1/2	1.414	2	1.570
2	CGLw	$\frac{1}{30}\xi^2$	$-\frac{2}{135}\xi^4$	$-\frac{1}{48}\xi^2$	1/2	0.426	$2/3 = 0.667$	0.541
3	CGLw	$\frac{9}{1280}\xi^4$	$-\frac{9}{320}\xi^4$	$-\frac{9}{5120}\xi^4$	1/2	0.213	0.354	0.297
4	CGLw	$-\frac{1}{405}\xi^4$	$-\frac{32}{4725}\xi^6$	$-\frac{1}{630}\xi^4$	1/2	0.132	0.224	0.192
5	CGLw	$-\frac{625}{344064}\xi^6$	$\frac{625}{258048}\xi^6$	$\frac{-625}{1032192}\xi^6$	1/2	0.0909	0.155	0.135
3	EQUI	see LGL	$-\frac{61}{1080}\xi^4$	$-\frac{42}{295}\xi^2$	0.651	see LGL	0.369	0.329
4	EQUI	see LGL	$\frac{40}{1137}\xi^4$	$\frac{56825}{157068}\xi^4$	(1.72)	see LGL	0.184	(0.173)
5	EQUI	see LGL	$\frac{-92807}{312500}\xi^4$	$\frac{33740850}{26406233}\xi^2$	(1.96)	see LGL	0.125	(0.117)

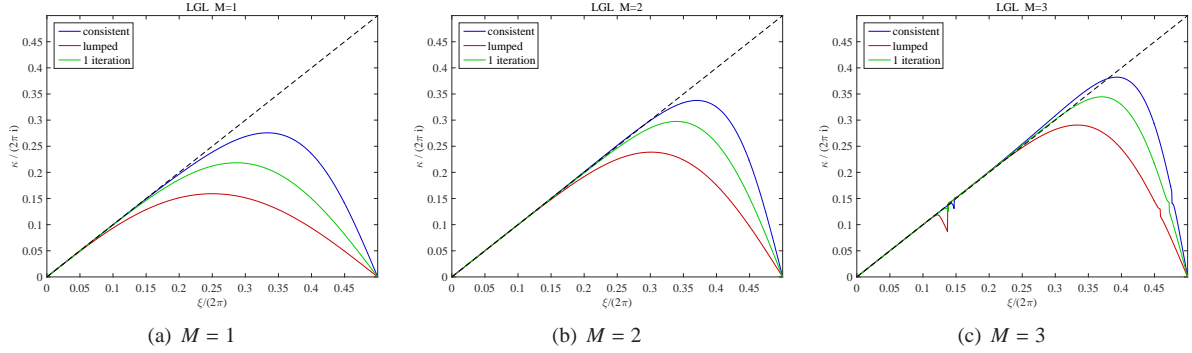


Figure 1: Dispersion curves for Legendre-Gauss-Lobatto points without and with mass lumping and after one iteration, for degree  $M = 1$  (a), 2 (b), and 3 (c).

### 3. Results

#### 3.1. Dispersion analysis

We compared the various spatial discretizations in terms of their dispersion curves, obtained by Fourier analysis, as well by set of numerical experiments. As an example, Fig. 1 shows dispersion curves for polynomials of degrees 1 to 3 on Legendre-Gauss-Lobatto points (LGL). Each graph shows the result without and with mass lumping as well as with 1 iteration of defect correction. The jumps in Fig. 1c are caused by the fact that in the Fourier analysis,  $M$  modes are considered simultaneously. Each of them corresponds to a particular root of the eigenvalue equation and can be assigned to a different wavenumber in the spectrum, according to how well the corresponding eigenvector matches the Fourier mode for that wavenumber [3].

With lumping, the deviation from the exact dispersion curve, the straight line, increases, but not so much at the smaller values of  $\xi$ . With one iteration of  $\mathcal{G} = I - (\mathcal{M}^L)^{-1}\mathcal{M}$ , the result is improved. For the smaller wavenumbers, we have analytically determined the asymptotic error behaviour by taking the leading term in the series expansion of  $\kappa/\xi - 1$  for the eigenvalue that is valid at small  $\xi$ . The results are listed in Table 1 for various cases. For degree  $M = 1$  and  $M = 2$ , the standard element (EQUI), the Legendre-Gauss-Lobatto points (LGL) and the unweighted Chebyshev-Gauss-Lobatto (CGL) points lead to the same discretization and, therefore, all provide the same results. The same is true when the consistent mass matrix is used. Then, the choice of nodes does not matter. The exception is the weighted scheme with Chebyshev-Gauss-Lobatto nodes (CGLw), where the weighting functions changes the

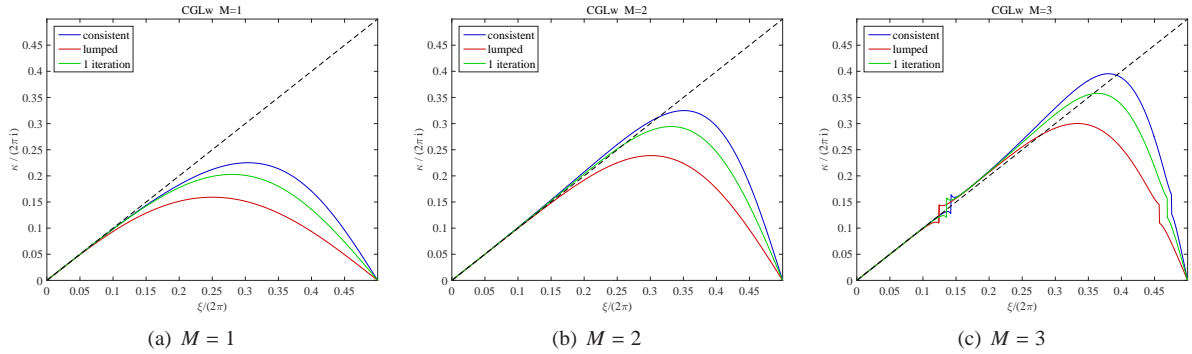


Figure 2: Dispersion curves for CGLw without and with mass lumping and after one iteration, for degree  $M = 1$  (a), 2 (b), and 3 (c).

outcome. Note that for the latter, the error analysis did *not* involve a weighted norm. Figure 2 show dispersion curves for degrees up to 3.

Interestingly, the LGL scheme without mass lumping has a fourth-order error instead of the usual second-order. In the finite-difference world, [13] found the same behaviour. Without lumping and just a single iteration, this fourth-order behaviour is recovered, albeit with a larger error constant and not necessarily on a finite-difference grid with constant mesh spacing.

With LGL and higher but odd degrees, 1 iteration reduces the size of the error but does not suffice to recover the super-convergence obtained with a consistent mass matrix. This appears to contradict the expected behaviour of the defect correction method, until one realized that for  $M > 1$ , there are  $M$  coupled modes, each representing a different point on the dispersion curve. This coupling is responsible for what are known as ‘spurious’ modes and apparently has a negative effect on the performance of the defect correction method.

For even degrees, the error constant changes after lumping but not the exponent. The error can be reduced by one or more iterations. Appendix B shows that the spectral radius of the iteration matrix obeys  $\rho(\mathcal{G}) = (M + 1)/(2M + 1)$ .

The CFL number that dictates the maximum allowable time step is listed in the last two columns. For degree 1, it is nearly twice as large after lumping. This will amply offset the cost of one iteration if the time stepping error does not dominate the problem. For higher degrees, the increase in CFL is not as dramatic.

A closed-form expression for the leading dispersion error with the consistent mass matrix and LGL points was found by [7] and is quoted in Appendix C. A conjecture for the lumped case is included. For odd  $M$ , the error is completely due to the mass lumping and the related expression for the leading error can be found in [3].

With Patera’s scheme (CGL), we do expect the mass lumping to lower the accuracy, as the choice of nodes for the unweighted case is not related to any type of accurate numerical quadrature. The application of a single iteration may completely ruin the formal accuracy and more iterations are required to repair the harm. The same happens in the standard case (EQU).

The behaviour of CGLw follows a regular pattern. Note that the weighted norm was not used in the analysis. Overall, errors are larger than with LGL. If  $M$  is odd, the lumping increases the error, but if  $M$  is even, lumping improves it and iterations will only increase the error. The spectral radius of the defect correction matrix does not depend on the degree of the element:  $\rho(\mathcal{G}) = 1/2$ , as shown in Appendix B.

One may wonder if diagonal preconditioning [9, e.g.] would perform in a similar way. As an example, we consider LGL for degree  $M = 3$  and let  $\mathcal{H} = I - (\text{diag}\{\mathcal{M}^L\})^{-1}\mathcal{M}$ . In the Fourier domain, we obtain eigenvalues between  $-\frac{1}{6}$  and  $\frac{1}{2}$ . After one iteration, the dispersion curve for small  $\xi$  behaves as  $\xi(1 - \frac{1}{36} - \frac{9}{1120}\xi^8)$ . The term with  $\frac{1}{36}$  actually destroys the formal accuracy, which needs to be repaired with subsequent iterations. We therefore expect diagonal preconditioning to be far less efficient than preconditioning with the mass-lumped mass matrix.

### 3.2. Error in the eigenvectors

The dispersion curves describe the errors in the eigenvalues. For  $M > 1$ , the error in eigenvectors also plays a role. To obtain that error, we compare to the exact eigenfunction  $\bar{\mathbf{w}}$ , which is of the form  $\bar{\mathbf{w}}_j = e^{2\pi i m x_j}$ , with  $x_j$  the node positions as defined above. The discrete problem has eigenvectors  $\mathbf{q}_l$ . We can express  $\bar{\mathbf{w}}$  as a the unique

Table 2: Exponents of the leading error in the dispersion curve and in the eigenvectors with LGL points and polynomials up to degree 5. The first of each pair corresponds to the relative error in the eigenvalue  $i\kappa$  for the first-order formulation or in the square root of the eigenvalue  $\kappa^2$  for the second-order formulation. The second corresponds to the exponent of  $\xi$  in the leading error of the matrix  $S$  describing the eigenvector errors. This error is zero for  $M = 1$ . The last column shows expressions for the trend for  $M > 1$ , suggested by these results, where  $p(M) = 2 \text{ floor}\{(M + 1)/2\}$ , that is,  $p(M) = M$  if  $M$  is even and  $p(M) = M + 1$  if  $M$  is odd.

order	mass matrix	$M = 1$	2	3	4	5	trend ( $M > 1$ )
1	consistent	4, -	4, 2	8, 4	8, 4	12, 6	$2p(M), p(M)$
	lumped	2, -	4, 2	6, 4	8, 4	10, 6	$2M, p(M)$
2	consistent	2, -	4, 4	6, 5	8, 6	10, 7	$2M, M + 2$
	lumped	2, -	4, 4	6, 5	8, 6	10, 7	$2M, M + 2$

Table 3: Numerical results for the  $L_\infty$ - and  $L_2$ -errors when taking the first derivative using Legendre polynomials and a consistent mass matrix. Listed are the exponents  $p$  of a power-law fit of the form  $ch^p$ , where  $h \propto 1/N_{\text{dof}}$ , to the  $L_\infty$ - or  $L_2$ -errors shown in Fig. 3. The second and third column were obtained for a uniform grid. The fourth and fifth columns were obtained for a mesh with an abrupt jump in mesh size halfway the domain. Columns six to ten show similar results, but with projection instead of sampling of the initial data and the exact solution. The sixth column, for  $L_\infty$  on a uniform mesh, now agrees with the first row of results in Table 2. On the non-uniform mesh, the convergence rates are worse.

mesh	sampling				projection			
	uniform		non-uniform		uniform		non-uniform	
$M$	$L_\infty$	$L_2$	$L_\infty$	$L_2$	$L_\infty$	$L_2$	$L_\infty$	$L_2$
1	4.0	4.5	1.0	2.0	4.0	4.5	1.0	2.0
2	2.0	2.5	2.0	2.5	2.0	2.5	1.9	2.5
3	3.0	3.5	3.0	3.5	4.0	4.6	3.0	4.2
4	4.0	4.5	3.9	4.5	3.9	4.4	3.9	4.4
5	5.0	5.5	5.0	5.5	6.1	6.6	5.1	6.3

linear combinations of these eigenvectors by  $\bar{\mathbf{w}} = \sum_{l=0}^{M-1} \psi_l \mathbf{q}_l$ . The error in the eigenvectors is given by the vectors  $\mathbf{r}_l = \psi_l \mathbf{q}_l - \bar{\mathbf{w}} \delta_{l=l_{\text{ref}}}$ ,  $l = 0, 1, \dots, M - 1$ . Here,  $\delta_{l=l_{\text{ref}}}$  is the Kronecker delta, which is zero except for  $l = l_{\text{ref}}$ , the index that corresponds to the ‘physical’ eigenvalue that approximates  $iM\xi$ . The other indices correspond to the ‘spurious’ modes. Instead of an absolute error, we can determine a relative error by dividing each vector  $\mathbf{r}_l$  element-wise by  $\bar{\mathbf{w}}$  to obtain  $\tilde{\mathbf{r}}_l$  with  $\tilde{r}_{l,j} = r_{l,j}/\bar{w}_j$ . The vectors  $\tilde{\mathbf{r}}_l$  can be combined into a matrix  $S$ , which has them as columns. This matrix describes the error in approximating the exact eigenfunction as well as the energy that is leaked into the ‘spurious’ modes.

In [3], the matrix  $S$  was determined in the Fourier domain, followed by an inverse Fourier transform. We can obtain the same results by working in the spatial domain, using the eigenvectors obtained by static condensation. Given the fact that these vectors are completely defined by their first  $M$  values for  $j_1 = 0, 1, \dots, M - 1$  at  $j_0 = 0$ , the matrix  $S$  will have size  $M \times M$ .

In Appendix D, we have listed the eigenvalue and eigenvector errors for polynomials up to degree  $M = 5$  and LGL points, both for the first-order formulation that is the subject of this paper and for the second-order formulation discussed elsewhere [3].

Table 2 summarizes the exponents of the leading errors in the eigenvalues and eigenvectors. The last column contains the suggested trends for  $M > 1$ , where it should be noted that exponents for the dispersion error in the second-order case were proven in [3] and later also in [4] and [5]. For the first-order case with a consistent mass matrix, a proof can be found in [7].

### 3.3. Numerical experiments

Before turning to the first-order formulation of the wave equation, we consider simple differentiation with the consistent mass matrix to verify the eigenvalue and eigenvector estimates. We consider the function  $p(x) = \frac{1}{2\pi m} \sin(2\pi mx)$  with  $m = 3$  on the periodic interval  $\xi \in [0, 1)$ . The mesh is either uniform with constant  $h = 1/N$  for  $N$  elements or with two different spacings  $h_L$  and  $h_R$ . In the last case, we set  $h_j = h_L$  for  $j = 0, \frac{1}{2}N - 1$ ,  $h_j = h_R$  for  $j = \frac{1}{2}N, N - 1$ , with  $N$  chosen even and  $h_L = 0.8h_R$ . Figure 3 shows the maximum error as a function of the reciprocal of the number

Table 4: As Table 3, but for the weighted Chebyshev polynomials. See also Fig. 4.

mesh $M$	sampling				projection			
	uniform		non-uniform		uniform		non-uniform	
	$L_\infty$	$L_2$	$L_\infty$	$L_2$	$L_\infty$	$L_2$	$L_\infty$	$L_2$
1	2.0	2.5	1.0	2.1	2.0	2.5	1.0	2.1
2	2.0	2.5	2.0	2.5	2.0	2.5	2.0	2.5
3	3.0	3.5	3.0	3.5	4.0	4.5	2.9	4.3
4	4.0	4.5	4.0	4.5	3.9	4.5	3.9	4.4
5	5.0	5.5	5.0	5.5	6.0	6.5	5.1	6.3

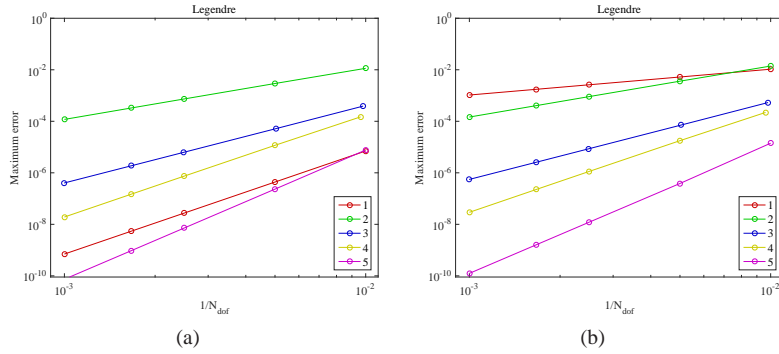


Figure 3: Maximum differentiation error for a simple test problem using Legendre polynomials as a function of the number of degrees of freedom,  $N_{\text{dof}}$ , for polynomial degrees 1 to 5. The grid spacing is either constant (a) or has an abrupt jump halfway the periodic domain (b).

of degrees of freedom,  $N_{\text{dof}}$ , for polynomial degrees 1 to 5. Power-law fits to the results provide the powers listed in Table 3. With pointwise sampling of the input function and the exact solution, the error behaviour is worse than the estimates of Table 2. With a proper projection on the basis function and a uniform mesh, the same powers are found for the  $L_\infty$  estimates. With the non-uniform mesh, the maximum error appears to behave as  $h^M$  and error cancellation and super-convergence are lost.

Similar results with weighted Chebyshev polynomials (CGLw) are shown in Fig. 4 and Table 4. Again, the odd degrees lead to a better performance.

These numerical results confirm that dispersion error analysis by itself is insufficient and that the eigenvector errors have to be included as well.

In addition to the above dispersion-curve analysis, we have performed a set of numerical experiments on the first-order formulation of the acoustic wave equation. We consider a Ricker pulse, the second time derivative of a Gaussian, travelling around once on a periodic domain.

We ran at a fraction of  $10^{-3}$  times the maximum time step dictated by the CFL condition to avoid too much imprint of the time stepping error. A less costly alternative would be to perform higher-order time stepping [14, 15, 16, 17] or dispersion correction [18, 19, 20].

As before, we used two difference spacing  $h_L$  and  $h_R$ . The standard deviation of the Ricker pulse was 0.0375 times the length of the domain. The initial and final position of its centre was at 0.74 of the length of the domain, in the part to the right that has the larger spacing.

Figure 5a–c plot the maximum errors in the particle velocity  $v(t_{\text{max}}, x)$  after one round trip for a varying number of degrees of freedom without and with mass lumping and with one extra iteration for polynomial degrees  $M = 1$  to 5. One iteration clearly pays off for the lowest degree,  $M = 1$ , and also for the higher degrees when the number of degrees of freedom is small and the error large. Overall, the effect of the eigenvector errors, summarized in Table 2, dominates the results for degrees larger than one. The improvement with defect correction is the largest for the lowest degree,  $M = 1$ . Although the fourth-order super-convergence for this degree is lost on a non-uniform mesh, the accuracy after 1 iteration is still considerably better than with just mass lumping.

In addition to the above runs, a few additional experiments were conducted to investigate how a larger number of

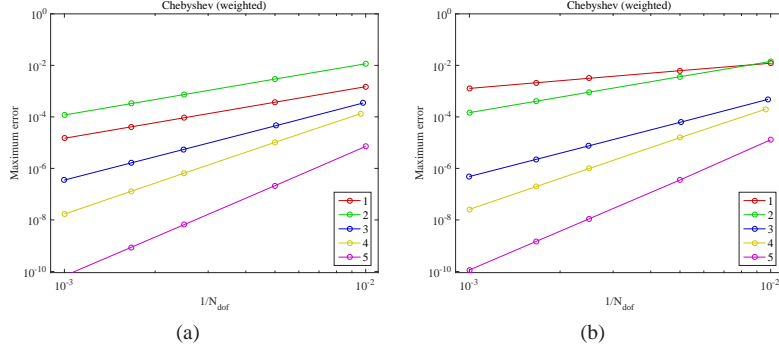


Figure 4: As Fig. 3, but for weighted Chebyshev polynomials (CGLw).

iterations affect the result and if a diagonal matrix would be a better preconditioner, as suggested by [9]. Figure 5e–f show the result of increasing the number of iterations with the operator  $\mathcal{G}$ , without attempting to obtain some acceleration with the conjugate gradient method. We observe a slight improvement, but the increase in computational costs hardly pays off.

Figure 6 shows results after using the diagonal of the mass matrix instead of the lumped mass matrix as preconditioner. It can be seen that in order for the  $\text{diag}(\mathcal{M})$  to behave similar to  $\mathcal{M}^L$ , at least 20 iterations are required, showing that the lumped mass matrix is superior as preconditioner.

Finally, Fig. 7 displays the error behaviour for CGLw. Note that the dispersion curves are based on the usual norm and do not involve weighting. Again, one iteration helps to improve the accuracy, as for LGL.

#### 4. Generalization to 2D

We can quickly analyze the performance in 2D by considering Fourier analysis on a periodic grid with square elements, both for bilinear elements and for linear elements on triangles.

We start with bilinear elements on squares. Let  $T_x$  denote a shift operator in the  $x$ -direction, such that  $T_x p_{k,l} = p_{k+1,l}$ . Here,  $p_{k,l}$  denotes the discrete pressure in the point  $(x_k, y_l)$  with  $x_k = x_0 + kh_x$  and  $y_l = y_0 + lh_y$  and grid spacings  $h_x$  and  $h_y$ . Its Fourier symbol is  $\hat{T}_x = \exp(i\xi_1)$  with  $|\xi_1| \leq \pi$ , where  $\xi_1$  is related to the wavenumber  $k_x$  in the  $x$ -direction by  $\xi_1 = k_x h_x$ . Likewise,  $T_y p_{k,l} = p_{k,l+1}$  with symbol  $\hat{T}_y = \exp(i\xi_2)$  with  $|\xi_2| \leq \pi$ . One row of the assembled mass matrix in a single node, relative to the others, is

$$\mathcal{M} = \frac{1}{36} \left[ 16 + 4(T_x^{-1} + T_x + T_y^{-1} + T_y) + T_x^{-1}T_y^{-1} + T_x T_y^{-1} + T_x^{-1}T_y + T_x T_y \right].$$

Its symbol is

$$\hat{\mathcal{M}} = \frac{1}{36} (\hat{T}_x^{-1} + 4 + \hat{T}_x) (\hat{T}_y^{-1} + 4 + \hat{T}_y) = \frac{1}{9} (2 + \cos \xi_1) (2 + \cos \xi_2).$$

One row of the derivative matrix in  $x$  is

$$\mathcal{D}^{(1)} = \frac{1}{12} (T_x - T_x^{-1}) (T_y^{-1} + 4 + T_y),$$

with symbol

$$\hat{\mathcal{D}}^{(1)} = \frac{2}{3} i (2 + \cos \xi_2) \sin \xi_1.$$

For  $\mathcal{D}^{(2)}$ , we can swap  $\xi_1$  and  $\xi_2$ . Then,

$$\hat{\mathcal{M}}^{-1} \hat{\mathcal{D}}^{(1)} = \frac{3i \sin \xi_1}{2 + \cos \xi_1} \simeq i \xi_1 \left( 1 - \frac{1}{180} \xi_1^4 \right),$$

showing that we have fourth-order accuracy with bilinear elements and a consistent mass matrix. With mass lumping, the result has only second-order accuracy:

$$\hat{\mathcal{M}}^L^{-1} \hat{\mathcal{D}}^{(1)} = \frac{1}{3} i (2 + \cos \xi_1) \sin \xi_1 \simeq i \xi_1 \left[ 1 - \frac{1}{6} (\xi_1^2 + \xi_2^2) \right].$$

The expressions can be used to estimate the eigenvalues of  $G$  by noting that

$$\hat{G} = 1 - \frac{1}{9}(2 + \cos \xi_1)(2 + \cos \xi_2) \in [0, \frac{8}{9}].$$

After one iteration with  $\hat{G}$ , the error becomes

$$-\frac{1}{180} (6\xi_1^4 + 10\xi_1^2\xi_2^2 + 5\xi_2^4),$$

restoring the fourth-order accuracy.

We can repeat this analysis for linear elements on triangles and a regular mesh consisting of squares cut in half across the diagonal, from the left upper to the right lower corner. With unit spacing, the first triangle has vertices  $(0, 0)$ ,  $(1, 0)$ ,  $(0, 1)$  with basis functions  $\{1 - x - y, x, y\}$  and the second has  $(1, 1)$ ,  $(1, 0)$ ,  $(0, 1)$  with basis functions  $\{-(1 - x - y), 1 - y, 1 - x\}$ . For the Fourier analysis, we select 8 triangles contained inside the 4 squares surrounding one node and assemble the matrices. Then, one row of the mass matrix is given by

$$\mathcal{M} = \frac{1}{12}(6 + T_x^{-1} + T_x + T_y^{-1} + T_y + T_x T_y^{-1} + T_x^{-1} T_y),$$

with corresponding symbol

$$\hat{\mathcal{M}} = \frac{1}{6}(3 + \cos \xi_1 + \cos \xi_2 + \cos(\xi_1 - \xi_2)).$$

A row of the  $x$ -derivative matrix is

$$\mathcal{D}^{(1)} = \frac{1}{6} [2(T_x - T_x^{-1}) + T_y(1 - T_x^{-1}) + T_y^{-1}(1 - T_x)],$$

with symbol

$$\hat{\mathcal{D}}^{(1)} = \frac{1}{3}i(2 \sin \xi_1 + \sin \xi_2 + \sin(\xi_1 - \xi_2)).$$

Now,

$$\hat{\mathcal{M}}^{-1} \hat{\mathcal{D}}^{(1)} \simeq i\xi_1 \left[ 1 - \frac{1}{360}\xi_1^2 \{2\xi_1^2 - 5\xi_2(\xi_1 - \xi_2)\} \right],$$

revealing fourth-order behaviour of the error. The results for the derivative in the  $y$ -direction are the same after swapping  $T_x$  and  $T_y$  or  $\xi_1$  and  $\xi_2$ . With mass lumping, the operator becomes

$$(\hat{\mathcal{M}}^L)^{-1} \hat{\mathcal{D}}^{(1)} = \hat{\mathcal{D}}^{(1)} \simeq i\xi_1 \left[ 1 - \frac{1}{6}(\xi_1^2 + \xi_2^2 - \xi_1 \xi_2) \right],$$

providing only second-order accuracy. These expressions also provide an estimate of the eigenvalue range of  $G$ :

$$\hat{G} = \frac{1}{6} [3 - \cos \xi_1 - \cos \xi_2 - \cos(\xi_1 - \xi_2)] \in [0, \frac{3}{4}].$$

One iteration with  $\hat{G}$  reduces the relative error to

$$-\frac{1}{360} (12\xi_1^4 - 25\xi_1^3\xi_2 + 35\xi_1^2\xi_2^2 - 20\xi_1\xi_2^3 + 10\xi_2^4),$$

again restoring the fourth-order accuracy.

It remains to be seen if this accuracy can actually be obtained in numerical experiments. A practical problem in seismic applications is the need to sample the wave field in arbitrary points of the computational domain. To reach a sufficiently high interpolation degree, the polynomials that represent the solution are not suited. Essentially non-oscillatory interpolation may provide a solution in that case [21, 22].

## 5. Conclusions

We have compared four finite-element schemes with polynomial basis functions for the first-order formulation of the acoustic wave equation, using Legendre-Gauss-Lobatto nodes, Chebyshev-Gauss-Lobatto without and with weighting function or the standard element. Mass lumping, desired for numerical efficiency since it allows for explicit time stepping, tends to decrease the spatial accuracy. The remaining accuracy in the numerical dispersion is best for the Legendre-Gauss-Lobatto nodes and, for polynomials of odd degrees, exceeds that of the second-order formulation

of the wave equation. In some cases, the accuracy can be improved by applying one iteration on the consistent mass matrix, preconditioned by its lumped version. For polynomials of degree one, this improves the accuracy from second to fourth order in the element size. In other cases, the improvement in accuracy is less dramatic.

The error in the eigenvectors for the first-order formulation, however, is worse than obtained for the second-order formulation, without and with mass lumping. Because the eigenvector error is zero for the lowest-degree scheme, with linear polynomials, our iterative approach appears to be most attractive for just that case.

Fourier analysis in two space dimensions suggests that the fourth-order error behaviour should be obtained for the lowest-order scheme, either with bilinear elements on quadrilaterals or with linear elements on triangles, at least on very regular meshes and with constant material properties. Whether or not this still holds on general unstructured meshes remains to be seen.

## Acknowledgements

This work is part of the research programme of the Foundation for Fundamental Research on Matter (FOM), which is part of the Netherlands Organisation for Scientific Research (NWO). The authors are indebted to Martin van Gijzen for helpful suggestions.

## References

- [1] W. A. Mulder, A comparison between higher-order finite elements and finite differences for solving the wave equation, in: J.-A. Désidéri, P. LeTalleca, E. Oñate, J. Périaux, E. Stein (Eds.), *Proceedings of the Second ECCOMAS Conference on Numerical Methods in Engineering*, Paris, Sept. 9–13, 1996, John Wiley & Sons, Chichester, 1996, pp. 344–350.
- [2] E. Zhebel, S. Minisini, A. Kononov, W. A. Mulder, A comparison of continuous mass-lumped finite elements with finite differences for 3-D wave propagation, *Geophysical Prospecting* 62 (5) (2014) 1111–1125. doi:10.1111/1365-2478.12138.
- [3] W. A. Mulder, Spurious modes in finite-element discretizations of the wave equation may not be all that bad, *Applied Numerical Mathematics* 30 (4) (1999) 425–445. doi:10.1016/S0168-9274(98)00078-6.
- [4] M. Ainsworth, Discrete dispersion relation for hp-version finite element approximation at high wave number, *SIAM Journal on Numerical Analysis* 42 (2) (2004) 553–575. doi:10.1137/S0036142903423460.
- [5] M. Ainsworth, H. A. Wajid, Dispersive and dissipative behavior of the spectral element method, *SIAM Journal on Numerical Analysis* 47 (5) (2009) 3910–3937. doi:10.1137/080724976.
- [6] G. Cohen, *Higher-Order Numerical Methods for Transient Wave Equations*, Springer, 2002.
- [7] M. Ainsworth, Dispersive behaviour of high order finite element schemes for the one-way wave equation, *Journal of Computational Physics* 259 (2014) 1–10. doi:10.1016/j.jcp.2013.11.003.
- [8] H. J. Stetter, The defect correction principle and discretization methods, *Numerische Mathematik* 29 (4) (1978) 425–443. doi:10.1007/BF01432879.
- [9] A. J. Wathen, Realistic eigenvalue bounds for the Galerkin mass matrix, *IMA Journal of Numerical Analysis* 7 (4) (1987) 449–457. doi:10.1093/imanum/7.4.449.
- [10] L. L. Thompson, P. M. Pinsky, Complex wavenumber Fourier analysis of the p-version finite element method, *Computational Mechanics* 13 (4) (1994) 255–275. doi:10.1007/BF00350228.
- [11] A. T. Patera, A spectral element method for fluid dynamics: Laminar flow in a channel expansion, *Journal of Computational Physics* 54 (3) (1984) 468–488. doi:10.1016/0021-9991(84)90128-1.
- [12] S. K. Lele, Compact finite difference schemes with spectral-like resolution, *Journal of Computational Physics* 103 (1) (1992) 16–42. doi:10.1016/0021-9991(92)90324-R.
- [13] P. Lax, B. Wendroff, Systems of conservation laws, *Communications on Pure and Applied Mathematics* 31 (2) (1960) 217–237. doi:10.1002/cpa.3160130205.
- [14] M. A. Dablain, The application of high-order differencing to the scalar wave equation, *Geophysics* 51 (1) (1986) 54–66. doi:10.1190/1.1442040.
- [15] G. R. Shubin, J. B. Bell, A modified equation approach to constructing fourth order methods for acoustic wave propagation, *SIAM Journal on Scientific and Statistical Computing* 8 (2) (1987) 135–151. doi:10.1137/0908026.
- [16] J. C. Gilbert, P. Joly, Higher order time stepping for second order hyperbolic problems and optimal CFL conditions, *Computational Methods in Applied Sciences* 16, Springer, Berlin, 2008, pp. 67–93.
- [17] C. Stork, Eliminating nearly all dispersion error from FD modeling and RTM with minimal cost increase, in: *75th EAGE Conference & Exhibition incorporating SPE EUROPEC*, Extended Abstract, 2013. doi:10.3997/2214-4609.20130478.
- [18] M. Wang, S. Xu, Time dispersion transforms in finite difference of wave propagation, in: *77th EAGE Conference & Exhibition*, Extended Abstract, 2015. doi:10.3997/2214-4609.201412619.
- [19] J. E. Anderson, V. Brytik, G. Ayeni, Numerical temporal dispersion corrections for broadband temporal simulation, RTM and FWI, in: *SEG Technical Program Expanded Abstracts*, 2015, pp. 1096–1100. doi:10.1190/segam2015-5817144.1.
- [20] A. Harten, B. Engquist, S. Osher, S. R. Chakravarthy, Uniformly high order accurate essentially non-oscillatory schemes, III, *Journal of Computational Physics* 71 (2) (1987) 231–303. doi:10.1016/0021-9991(87)90031-3.

- [21] M. Putti, W. W.-G. Yeh, W. A. Mulder, A triangular finite volume approach with high resolution upwind terms for the solution of groundwater transport equations, *Water Resources Research* 26 (12) (1990) 2865–2880.
- [22] P. Joly, Variational methods for time-dependent wave propagation problems, in: M. Ainsworth, P. Davies, D. Duncan, B. Rynne, P. Martin (Eds.), *Topics in Computational Wave Propagation: Direct and Inverse Problems*, Springer, Berlin, Heidelberg, 2003, pp. 201–264. doi:10.1007/978-3-642-55483-4\_6.
- [23] S. Geršgorin, Über die Abgrenzung der Eigenwerte einer Matrix, *Bulletin de l'Académie des Sciences de l'URSS. Classe des sciences mathématiques et naturelles* 6 (1931) 749–754.
- [24] S. A. Teukolsky, Short note on the mass matrix for Gauss-Lobatto grid points, *Journal of Computational Physics* 283 (2015) 408–413. doi:10.1016/j.jcp.2014.12.012.
- [25] D. Funaro, *Polynomial Approximations of Differential Equations*, Lecture Notes in Physics. New Series m: Monographs, Vol. 8, Springer-Verlag, Berlin, 1992.

## Appendix A. Time-stepping stability

We examine the stability of the the time-stepping scheme (1) by considering a discrete energy. Weighted scalar products on the 1-D domain  $\Omega$  are defined by

$$(p, q)_p = \int_{\Omega} w_p(x)p(x)q(x)dx, \quad (v, u)_v = \int_{\Omega} w_v(x)v(x)u(x)dx,$$

for the pressure and velocity, respectively. The domain is partitioned into  $K$  elements, each with  $M + 1$  nodes. For the velocity at time  $n$ , we use the representation  $v^n = \sum_{k=1}^K \sum_{\ell=1}^M v_{k,\ell}^n \phi_{k,\ell}(x)$  with  $k$  running over the elements and  $\ell$  over the  $M + 1$  nodes of each element. On a periodic mesh, the index  $\ell = 0$  on an element refers to the same node as  $\ell = M$  of its left neighbour. Likewise, we let  $p^{n+1/2} = \sum_{k=1}^K \sum_{\ell=1}^M p_{k,\ell}^{n+1/2} \psi_{k,\ell}(x)$ . With this, we have

$$(v^n, u^n)_v = (\mathbf{v}^n)^\top \mathcal{M}_v \mathbf{u}^n, \quad (p^{n+1/2}, q^{n+1/2})_p = (\mathbf{p}^{n+1/2})^\top \mathcal{M}_p \mathbf{q}^n,$$

in terms of the mass matrices  $\mathcal{M}_v$  and  $\mathcal{M}_p$ .

The discrete energy can be defined as [23]

$$\mathcal{E}^n = \frac{1}{2}(v^n, v^n)_v + \frac{1}{2}(p^{n+1/2}, p^{n-1/2})_p.$$

With  $p^n \equiv \frac{1}{2}(p^{n+1/2} + p^{n-1/2})$ , it can be expressed as

$$\mathcal{E}^n = \frac{1}{2}(v^n, v^n)_v + \frac{1}{2}(p^n, p^n)_p - \frac{1}{4}(\Delta t)^2 \left( \frac{p^{n+1/2} - p^{n-1/2}}{\Delta t}, \frac{p^{n+1/2} - p^{n-1/2}}{\Delta t} \right)_p. \quad (\text{A.1})$$

Energy is conserved if

$$0 = \mathcal{E}^{n+1} - \mathcal{E}^n = \frac{1}{2}(v^{n+1} + v^n, v^{n+1} - v^n)_v + \frac{1}{2}(p^{n+1/2}, p^{n+3/2} - p^{n-1/2})_p =$$

$$\frac{1}{2}\Delta t \left\{ (\mathbf{v}^{n+1} + \mathbf{v}^n)^\top \mathcal{D}_p \mathbf{p}^{n+1/2} + (\mathbf{p}^{n+1/2})^\top \mathcal{D}_v (\mathbf{v}^{n+1} + \mathbf{v}^n) \right\} = \frac{1}{2}\Delta t (\mathbf{v}^{n+1/2})^\top (\mathcal{D}_p + \mathcal{D}_v^\top) \mathbf{p}^{n+1/2},$$

where  $\mathbf{v}^{n+1/2} = \frac{1}{2}(\mathbf{v}^n + \mathbf{v}^{n+1})$ . This requires  $\mathcal{D}_p = -\mathcal{D}_v^\top$ , which is the case for LGL, CGL, and EQUI on a periodic mesh, as these scheme have  $\mathcal{D}_p = -\mathcal{D}_p^\top$  and we have taken  $\mathcal{D}_v = \mathcal{D}_p$ . For CGLw, however, this is not true.

The discrete energy is non-negative for

$$\frac{4}{(\Delta t)^2} \geq \max_{\mathbf{v} \neq 0, \mathbf{p}} \frac{(\mathbf{v}^n)^\top \mathcal{D}_v^\top \mathcal{M}_p^{-1} \mathcal{D}_v \mathbf{v}^n}{(\mathbf{v}^n)^\top \mathcal{M}_v \mathbf{v}^n + (\mathbf{p}^n)^\top \mathcal{M}_p \mathbf{p}^n} \geq \max_{\mathbf{v} \neq 0} \frac{\mathbf{v}^\top \mathcal{D}_v^\top \mathcal{M}_p^{-1} \mathcal{D}_v \mathbf{v}}{\mathbf{v}^\top \mathcal{M}_v \mathbf{v}}$$

With  $\tilde{\mathbf{v}} = \mathcal{M}_v^{1/2} \mathbf{v}$ , this becomes

$$\frac{4}{(\Delta t)^2} \geq \max_{\tilde{\mathbf{v}} \neq 0} \frac{\tilde{\mathbf{v}}^\top \mathcal{L} \tilde{\mathbf{v}}}{\tilde{\mathbf{v}}^\top \tilde{\mathbf{v}}}, \quad \mathcal{L} = (\mathcal{M}_v^{-1/2})^\top \mathcal{D}_v^\top \mathcal{M}_p^{-1} \mathcal{D}_v \mathcal{M}_v^{-1/2}$$

or

$$\Delta t \leq \frac{2}{\sqrt{\rho(\mathcal{L})}}, \quad \mathcal{L} = (\mathcal{M}_p^{-1/2} \mathcal{D}_v \mathcal{M}_v^{-1/2})^\top (\mathcal{M}_p^{-1/2} \mathcal{D}_v \mathcal{M}_v^{-1/2}).$$

The similarity transform

$$\tilde{\mathcal{L}} = \mathcal{M}_v^{-1/2} \mathcal{L} \mathcal{M}_v^{1/2} = \mathcal{M}_v^{-\top} \mathcal{D}_v^\top \mathcal{M}_p^{-1} \mathcal{D}_v$$

does not alter the eigenvalues of  $\mathcal{L}$ . As LGL, CGL, and EQUI have  $\mathcal{M}_v = \mathcal{M}_p = \mathcal{M}$  and  $\mathcal{D}_v = \mathcal{D}_p = -\mathcal{D}_p^\top = \mathcal{D}$  on a 1-D periodic mesh, examining the eigenvalues of  $\tilde{\mathcal{L}} = -\mathcal{M}^{-1} \mathcal{D} \mathcal{M}^{-1} \mathcal{D}$  will suffice.

This leaves the question of the stability CGLW. Elimination of the velocity from the time-stepping equations (1) leads to

$$\frac{\mathbf{p}^{n+3/2} - 2\mathbf{p}^{n+1/2} + \mathbf{p}^{n-1/2}}{\Delta t^2} = -\bar{\mathcal{L}} \mathbf{p}^{n+1/2}, \quad \bar{\mathcal{L}} = -\mathcal{M}^{-1} \mathcal{D} \mathcal{M}^{-1} \mathcal{D}.$$

For CGLW, the matrix  $\tilde{\mathcal{L}}$  is not symmetric. However, numerical evidence shows that its eigenvalues are non-negative and bounded and that the time-stepping scheme therefore should be stable in 1D. Note that this does not guarantee stability in 2D, as non-symmetric matrices with non-negative eigenvalues are not necessarily non-negative themselves, and vice versa. Addition of two such matrices may lead to instabilities. Given the limited interest of the method, we have not further investigated its stability properties.

## Appendix B. Spectral radius of $G$

The spectral radius of  $\mathcal{G} = I - (\mathcal{M}^L)^{-1} \mathcal{M}$ , with mass matrix  $\mathcal{M}$  and its lumped version  $\mathcal{M}^L$ , should be smaller than 1 for convergence. Here, we provide estimates on a periodic domain with  $N$  elements, each with size  $h_j$ ,  $j = 0, \dots, N-1$ . The basis functions have degree  $M$ .

We start with some simple observations. The vector consisting of all ones is an eigenvector of  $\mathcal{G}$  with eigenvalue 0. This follows immediately from the fact that  $\mathcal{M}^L$  is a diagonal matrix obtained from the row sums of  $\mathcal{M}$ . The eigenvalues of  $G$  do not change under the similarity transform  $(\mathcal{M}^L)^{1/2} \mathcal{G} (\mathcal{M}^L)^{-1/2}$ . Since this is a symmetric matrix, its eigenvalues should be non-negative. Note that  $\mathcal{M}^L$  has positive entries on the diagonal.

For the lowest degree,  $M = 1$ , the mass matrix per element is

$$A = \frac{1}{6} \begin{pmatrix} 2 & 1 \\ 1 & 2 \end{pmatrix},$$

and the assembled mass matrix is of the form  $\mathcal{M}_{j,j-1} = \frac{1}{6} h_{j-1}$ ,  $\mathcal{M}_{j,j} = \frac{1}{3} (h_{j-1} + h_j)$ ,  $\mathcal{M}_{j,j+1} = \frac{1}{6} h_j$ , and zero otherwise. In the periodic case, the  $j$  should be interpreted as  $j \bmod N$ . Then,

$$\mathcal{G}_{j,j-1} = -\frac{1}{3} \frac{h_{j-1}}{h_{j-1} + h_j}, \quad \mathcal{G}_{j,j} = \frac{1}{3}, \quad \mathcal{G}_{j,j+1} = -\frac{1}{3} \frac{h_j}{h_{j-1} + h_j},$$

and zero otherwise. In the equidistant case with constant  $h_j$ , the eigenfunctions are  $\mathbf{q}_k$ ,  $k = 0, \dots, N-1$ , with  $q_{k,l} = \exp(2\pi i k l / N)$ ,  $l = 0, \dots, N-1$ . The corresponding eigenvalues are  $\frac{1}{3} [1 - \cos(2\pi k / N)]$ . Therefore, the eigenvalues of  $\mathcal{G}$  lie in the interval  $[0, 2/3]$ .

In the non-equidistant case, Gershgorin's theorem [24] can be applied:  $|\lambda - g_{i,i}| \leq \sum_{j \neq i} |g_{i,j}|$  leads to  $|\lambda - \frac{1}{3}| = \frac{1}{3}$ , implying  $0 \leq \lambda \leq 2/3$ , which are the same bounds as in the equidistant case.

### Legendre polynomials

We now turn to the general case,  $M \geq 1$ . The mass matrix for a single element in modal form is defined by  $A_{k,l}^m = \int_{-1}^1 w(\zeta) \psi_k(\zeta) \psi_l(\zeta)$  with a weighting function  $w(x)$  and modal basis functions  $\psi_k(\zeta)$ ,  $k = 0, \dots, M$ . The lumped mass matrix in nodal form is  $2W$ , where  $W = \text{diag}\{w_0, w_1, \dots, w_M\}$  is diagonal with  $w_0 = w_M = 1/[M(M+1)]$  and  $w_j = 1/[M(M+1)P_M(x_j)^2]$  for  $j = 1, \dots, M-1$ .

For Legendre polynomials, this results in a diagonal matrix with  $A_{j,j}^m = 1/(j + \frac{1}{2})$ ,  $j = 0, \dots, M$ . To obtain its nodal representation  $A^n = F^n A^m$ , we take the Legendre-Gauss-Lobatto (LGL) points  $\zeta_j$  that are the roots of  $(1 - \zeta^2) \frac{d}{d\zeta} P_M(\zeta) = 0$ .

The modal-to-nodal map  $F^n = (F^m)^{-1}$  with  $F_{k,l}^m = \psi_k(\zeta_l)$ , for  $k, l = 0, \dots, M$ . This can be expressed in closed form as [25, e.g.]

$$F_{j,k}^n = \frac{2w_j}{\gamma_k} \psi_k(\zeta_j), \quad 2w_j = A_{j,j}^L, \quad \gamma_k = 2 \sum_{j=0}^M w_j \psi_k^2(\zeta_j).$$

Here,  $\gamma_k = 1/(k + \frac{1}{2})$  for  $k = 0, \dots, M-1$  and  $\gamma_M = 2/M$  with the LGL nodes. Note that the numerical quadrature weights  $w_j$  should not be confused with the weighting function  $w(\zeta)$ .

The nodal form of the basis functions is  $\phi = F^n \psi$ . We have  $\phi_k(\zeta_l) = \delta_{k,l}$  by definition and  $\psi_k(\zeta) = \sum_{l=0}^M \psi_k(\zeta_l) \phi_l(\zeta)$ . This is the same as the earlier  $F^m \phi$ .

The lumped version of  $A^n$  is  $A^L$ , a diagonal matrix obtained from the row sums:  $A_{k,k}^L = \sum_{l=0}^M A_{k,l}^n$ . The latter are proportional to the LGL quadrature weights:

$$w_k = \frac{1}{2} A_{k,k}^L = \left[ M(M+1) (P_M(\zeta_k))^2 \right]^{-1}.$$

The difference between the mass matrices is expressed by

$$(A^L - A^n)_{j,k} = \left( \frac{2}{\gamma_M} \right)^2 \left( \gamma_M - \frac{1}{M + \frac{1}{2}} \right) w_j w_k P_M(\zeta_j) P_M(\zeta_k),$$

where  $\gamma_M = 2/M$ , so

$$(A^L - A^n)_{j,k} = \frac{2M(1+M)}{2M+1} w_j w_k P_M(\zeta_j) P_M(\zeta_k).$$

Define a vector  $\mathbf{f}$  with  $f_k = w_k P_M(\zeta_k)$ . Then  $A^L - A^n = \frac{2M(1+M)}{2M+1} \mathbf{f} \mathbf{f}^T$ . We immediately obtain an eigenvector  $\mathbf{f}$ . Since

$$\begin{aligned} \mathbf{f} \cdot \mathbf{f} &= \sum_{k=0}^M [w_k P_M(\zeta_k)]^2 = \sum_{k=0}^M \left( \frac{P_M(\zeta_k)}{M(M+1)[P_M(\zeta_k)]^2} \right)^2 = \\ &= \frac{1}{M(M+1)} \sum_{k=0}^M w_k = \frac{1}{M(M+1)}, \end{aligned}$$

the corresponding eigenvalue is  $\frac{2}{2M+1}$ . The other eigenvalues are zero because the matrix has rank 1.

Next, consider the matrix  $G = (A^L)^{-1} (A^L - A^n) = \frac{2M(1+M)}{2M+1} (A^L)^{-1} \mathbf{f} \mathbf{f}^T$ . As

$$\mathbf{f}^T (A^L)^{-1} \mathbf{f} = \frac{1}{2} \sum_{k=0}^M w_k (P_M(\zeta_k))^2 = \frac{1}{2M},$$

the matrix has an eigenvector  $\mathbf{q} = 2(A^L)^{-1} \mathbf{f}$  with entries  $q_k = P_M(\zeta_k)$  and the corresponding eigenvalue is  $\lambda_{\max} = (M+1)/(2M+1)$ . The other eigenvalues are zero, as before.

To go from this result to the assembled case, we follow [9]. The bounds of the eigenvalues,  $\lambda$ , obey

$$\min_{\mathbf{x} \neq 0} \frac{\mathbf{x}^T (\mathcal{M}^L - \mathcal{M}) \mathbf{x}}{\mathbf{x}^T \mathcal{M}^L \mathbf{x}} \leq \lambda \leq \max_{\mathbf{x} \neq 0} \frac{\mathbf{x}^T (\mathcal{M}^L - \mathcal{M}) \mathbf{x}}{\mathbf{x}^T \mathcal{M}^L \mathbf{x}},$$

For boolean matrix  $L$  represents the local-to-global map that take  $(M+1)$  unknowns on the  $N$  elements to the global  $MN$  unknowns. Then,

$$\min_{\mathbf{x} \neq 0} \frac{\mathbf{x}^T L^T (A^L - A^n) L \mathbf{x}}{\mathbf{x}^T L^T A^L L \mathbf{x}} \leq \lambda \leq \max_{\mathbf{x} \neq 0} \frac{\mathbf{x}^T L^T (A^L - A^n) L \mathbf{x}}{\mathbf{x}^T L^T A^L L \mathbf{x}},$$

which after setting  $\mathbf{y} = L \mathbf{x}$ , results in

$$\min_{\mathbf{y} \neq 0} \frac{\mathbf{y}^T (A^L - A^n) \mathbf{y}}{\mathbf{y}^T A^L \mathbf{y}} \leq \lambda \leq \max_{\mathbf{y} \neq 0} \frac{\mathbf{y}^T (A^L - A^n) \mathbf{y}}{\mathbf{y}^T A^L \mathbf{y}}.$$

Let  $\mathbf{y}' = (A^L)^{1/2}\mathbf{y}$ , using the fact that  $A^L$  is diagonal with positive entries on the diagonal. Then,

$$\min_{\mathbf{y}' \neq 0} \frac{(\mathbf{y}')^\top (A^L)^{-1/2} (A^L - A^n) (A^L)^{-1/2} \mathbf{y}'}{(\mathbf{y}')^\top \mathbf{y}'} \leq \lambda \leq \max_{\mathbf{y}' \neq 0} \frac{(\mathbf{y}')^\top (A^L)^{-1/2} (A^L - A^n) (A^L)^{-1/2} \mathbf{y}'}{(\mathbf{y}')^\top \mathbf{y}'}$$

The bounds follow from the smallest and largest eigenvalues of  $(A^L)^{-1/2}(A^L - A^n)(A^L)^{-1/2}$ , which by a similarity transform based on  $(A^L)^{1/2}$  are the same as those of  $(A^L)^{-1}(A^L - A^n)$ , namely zero and  $\lambda_{\max} = (M+1)/(2M+1)$ .

Note that  $\mathcal{G}$  has  $N(M-1)$  zero and  $N$  non-zero eigenvalues, reflecting the fact that the element matrix  $A^L - A^n$  has rank 1.

For even  $M$ , the maximum eigenvalue is obtained for a vector  $\mathbf{v}$  obtained from chaining the highest modal function  $P_M(\zeta)$  over the nodes. Consider an indexing function  $q(j, k) = (Mj + k) \bmod MN$  that enumerates the  $MN$  degrees of freedom on a periodic grid with elements  $j = 0, \dots, N-1$  and nodes per element  $k = 0, \dots, M$ . The vector  $\mathbf{v}$  has elements  $v_{q(j,k)} = P_M(\zeta_k^{LGL})$ , the highest degree Legendre polynomial evaluated at the LGL nodes  $\zeta_k^{LGL}$ . Recall that  $G$  refers to a single element and does not contain the element size. Therefore, the subset  $\mathcal{G}_{q(j,k_1), q(j,k_2)} = G_{k_1, k_2}$ , corresponding to the interior nodes with  $k_1 = 1, \dots, M-1$  and  $k_2 = 0, \dots, M$ , does not depend on the element size  $h_j$ . At the endpoints, we have  $\mathcal{G}_{q(j,0), q(j,0)-l} = \frac{h_{j-1}}{h_{j-1}+h_j} G_{0,l}$  and  $\mathcal{G}_{q(j,0), q(j,0)+l} = \frac{h_j}{h_{j-1}+h_j} G_{0,l}$  for  $l = 1, \dots, M$ , whereas  $\mathcal{G}_{q(j,0), q(j,0)} = G_{0,0}$ . Since for even values of  $M$ , the corresponding  $\mathbf{v}$  is symmetric according to  $v_{q(j,l)} = v_{q(j,-l)}$ , for  $l = 1, \dots, M$ , we find that  $\mathcal{G}\mathbf{v} = \lambda_{\max}\mathbf{v}$ .

For  $M$  odd but  $N$  even, we can do the same, but since  $P_M(-1) = -1$  in that case, a minus sign needs to be applied in alternating elements:  $v_{q(j,k)} = (-1)^j P_M(\zeta_k^{LGL})$ . Note that application of a minus sign has the effect of reversal of the order:  $P_M(\zeta_{M-k}^{LGL}) = -P_M(\zeta_k^{LGL})$  for  $k = 0, \dots, M$ . With this vector, the same approach as above leads to  $\mathcal{G}\mathbf{v} = \lambda_{\max}\mathbf{v}$ .

### Chebyshev polynomials

The weighting function can be taken as  $w(\zeta) = \frac{2}{\pi}(1 - \zeta^2)^{-1/2}$ , with an extra factor  $2/\pi$  to integrate a unit constant to 2, as in the case of the Legendre polynomials. The modal basis functions are  $\psi_k(\zeta) = T_k(\zeta) = \cos(k \arccos \zeta)$ ,  $k = 0, \dots, M$ , and the Chebyshev-Gauss-Lobatto (CGL) nodes  $\zeta_l = -\cos(\pi l/M)$ ,  $l = 0, \dots, M$ . The modal-to-nodal map has entries

$$F_{j,k}^n = (-1)^k 2M w_j w_k \cos(\pi jk/M),$$

with  $w_j = 1/M$ , for  $j = 1, \dots, M-1$  and  $w_0 = w_M = 1/(2M)$  [26, eq. 3.5.6]. The mass matrix in model form is  $A^m = \text{diag}\{2, 1, \dots, 1\}$ , which represents the orthogonality of the Chebyshev polynomials. For its lumped version, we can show that  $F^m A^L (F^m)^\top = \text{diag}\{2, 1, \dots, 1, 2\}$ . Knowing that numerical quadrature with the CGL nodes is exact for polynomials up to degree  $2M-1$ , we expect that the non-zero eigenvector can be represented by the modal basis function of highest degree, evaluated at the CGL nodes. If this is expressed as  $\mathbf{q}$  with entries  $q_j = T_M(\zeta_j) = (-1)^{M-j}$ ,  $j = 0, \dots, M$ , then  $(F^n \mathbf{q})_j = \delta_{j,M}$ . From this, it follows that  $(A^L - A^n)\mathbf{q} = F^n \text{diag}\{0, 0, \dots, 0, 1\} F^n \mathbf{q} = \frac{1}{2} F^n \text{diag}\{2, 1, \dots, 1, 2\} F^n \mathbf{q} = \frac{1}{2} A^L \mathbf{q}$ . Using the same approach of [9] as before, this implies that the eigenvalues of  $\mathcal{G}$  lie between 0 and  $1/2$ .

### Appendix C. Leading dispersion errors for LGL

The leading error term in the dispersion curve for the Legendre polynomials without lumping can be found in [7, eq. (14)]. In our notation and after division by  $iM\xi$ , this provides

$$\varepsilon_C \sim \frac{1}{2} (-1)^M \left( \frac{M!}{(2M+1)!} \right)^2 \begin{cases} \frac{M+1}{2M+3} (M\xi)^{2(M+1)} & \text{if } M \text{ odd,} \\ \frac{2M+1}{M+1} (M\xi)^{2M} & \text{if } M \text{ even.} \end{cases} \quad (\text{C.1})$$

With mass lumping and the LGL points, we conjecture that the leading error term is

$$\varepsilon_L \sim -\frac{(M\xi)^{2M}}{2M+1} \left( \frac{M!}{(2M)!} \right)^2 \left( \frac{M}{M+1} \right)^{(-1)^M}. \quad (\text{C.2})$$

We have verified this last result up to  $M = 10$ . For odd  $M$ , this matches the very last equation in [3], which describes the error caused by replacing the consistent mass matrix by its lumped version. For even  $M$ ,  $\varepsilon_L = -2M \varepsilon_C$ .

#### Appendix D. Leading eigenvector errors

In the following, we will present expressions for the discrete dispersion and for eigenvector errors. For the mass matrix, the consistent and lumped versions are considered. We only consider Legendre polynomials up to degree  $M = 5$  and Legendre-Gauss-Lobatto (LGL) nodes. For reference, results for the second-order formulation of the wave equations are included, for which some can be also found elsewhere [3]. For the first-order case, the eigenvalues of the discrete operator are  $iM\kappa$ . For the second-order case, they are  $\kappa^2$  and we list only the non-negative values of  $\kappa$ . Because the analytic expressions rapidly become quite complicated, only results in the form of leading terms in a series representation in terms of the normalized wavenumber  $\xi \in [-\pi, \pi]$  are given. Since for polynomials of degree  $M$ ,  $M$  modes are coupled if elements of constant size and constant material parameters are considered, the eigenvalues come in groups of  $M$  elements and the corresponding eigenvector errors can be represented by the  $M$  columns of the matrix  $S$ , as explained in Section 3.2. Among the  $M$  eigenvalues, one corresponds to the ‘physical’ eigenvalue that approximates  $iM\xi$  in the first-order or  $(M\xi)^2$  in the second-order formulation. The eigenvector error is absent and therefore zero for degree  $M = 1$ . For the higher degrees, a zero entry in the matrix should be read as  $o(\xi^p)$ , with  $p$  the power of  $\xi$  pulled out in front of the matrix.

$M = 1$ , LGL, first-order, consistent mass matrix:

$$\kappa = \frac{3 \sin \xi}{2 + \cos \xi} \sim \xi \left(1 - \frac{1}{180} \xi^4\right), \quad S = 0.$$

$M = 1$ , LGL, first-order, lumped mass matrix:

$$\kappa = \sin \xi \sim \xi \left(1 - \frac{1}{6} \xi^2\right), \quad S = 0.$$

$M = 1$ , LGL, second-order, consistent mass matrix:

$$\kappa = \sqrt{\frac{6(1 - \cos \xi)}{2 + \cos \xi}} \sim \xi \left(1 + \frac{1}{24} \xi^2\right), \quad S = 0.$$

$M = 1$ , LGL, second-order, lumped mass matrix:

$$\kappa = \sqrt{2(1 - \cos \xi)} \sim \xi \left(1 - \frac{1}{24} \xi^2\right), \quad S = 0.$$

$M = 2$ , LGL, first-order, consistent mass matrix:

$$\kappa = -\frac{\sin(\xi) \left(2 \cos \xi \mp \sqrt{10 - \cos^2 \xi}\right)}{2 - \cos^2 \xi} \sim \left\{-5\xi, \xi \left(1 + \frac{1}{270} \xi^4\right)\right\}, \quad S = S^{\text{F2C}} \sim \frac{\xi^2}{36} \begin{pmatrix} -2 & 2 \\ 1 & -1 \end{pmatrix}.$$

$M = 2$ , LGL, first-order, lumped mass matrix:

$$\kappa = -\frac{1}{2} \sin \xi \left(\cos \xi \mp \sqrt{8 + \sin^2 \xi}\right) \sim \left\{-2\xi, \xi \left(1 - \frac{2}{135} \xi^4\right)\right\}, \quad S = S^{\text{F2L}} \sim 2 S^{\text{F2C}}.$$

$M = 2$ , LGL, second-order, consistent mass matrix:

$$\kappa \sim \left\{\xi \left(1 + \frac{1}{90} \xi^4\right), \sqrt{15}\right\}, \quad S = S^{\text{S2C}} \sim -\frac{\xi^4}{360} \begin{pmatrix} -2 & 2 \\ 1 & -1 \end{pmatrix}.$$

$M = 2$ , LGL, second-order, lumped mass matrix:

$$\kappa \sim \left\{\xi \left(1 - \frac{1}{180} \xi^4\right), \sqrt{6}\right\}, \quad S = S^{\text{S2L}} \sim -5 S^{\text{S2C}}.$$

$M = 3$ , LGL, first-order, consistent mass matrix:

$$\kappa \sim \left\{ -\sqrt{\frac{14}{3}}, \xi \left( 1 - \frac{81}{39200} \xi^8 \right), \sqrt{\frac{14}{3}} \right\},$$

$$S = S^{\text{F3C}} \sim \frac{27}{28000} \xi^4 \begin{pmatrix} 25 & -50 & 25 \\ -5 - i\sqrt{210} & 10 & -5 + i\sqrt{210} \\ -5 + i\sqrt{210} & 10 & -5 - i\sqrt{210} \end{pmatrix}.$$

$M = 3$ , LGL, first-order, lumped mass matrix:

$$\kappa \sim \left\{ -\sqrt{\frac{10}{3}}, \xi \left( 1 - \frac{27}{2800} \xi^6 \right), \sqrt{\frac{10}{3}} \right\},$$

$$S \sim \frac{9}{800} \xi^4 \begin{pmatrix} 5 & -10 & 5 \\ -1 - i\sqrt{6} & 2 & -1 + i\sqrt{6} \\ -1 + i\sqrt{6} & 2 & -1 - i\sqrt{6} \end{pmatrix}.$$

$M = 3$ , LGL, second-order, consistent mass matrix:

$$\kappa \sim \left\{ \xi \left( 1 + \frac{81}{22400} \xi^6 \right), \sqrt{\frac{14}{3}}, \sqrt{\frac{20}{3}} \right\}, \quad S = S^{\text{S3C}} \sim i \frac{81\sqrt{5}}{35000} \xi^5 \begin{pmatrix} 0 & 0 & 0 \\ 1 & -1 & 0 \\ -1 & 1 & 0 \end{pmatrix}.$$

$M = 3$ , LGL, second-order, lumped mass matrix:

$$\kappa \sim \left\{ \xi \left( 1 - \frac{27}{22400} \xi^6 \right), \sqrt{\frac{10}{3}}, \sqrt{\frac{20}{3}} \right\}, \quad S = S^{\text{S3L}} \sim -\frac{7}{3} S^{\text{S4C}}.$$

$M = 4$ , LGL, first-order, consistent mass matrix:

$$\kappa \sim \left\{ -\sqrt{\frac{21}{8}}, -9\xi, \xi \left( 1 + \frac{128}{496125} \xi^8 \right), \sqrt{\frac{21}{8}} \right\}, \quad S = S^{\text{F4C}} \sim \frac{1}{3675} \xi^4 \begin{pmatrix} 0 & 56 & -56 & 0 \\ 0 & -24 & 24 & 0 \\ 0 & 21 & -21 & 0 \\ 0 & -24 & 24 & 0 \end{pmatrix}.$$

$M = 4$ , LGL, first-order, lumped mass matrix:

$$\kappa \sim \left\{ -\sqrt{\frac{21}{8}}, -4\xi, \xi \left( 1 - \frac{1024}{496125} \xi^8 \right), \sqrt{\frac{21}{8}} \right\}, \quad S = S^{\text{F4L}} \sim 2 S^{\text{F4C}}.$$

$M = 4$ , LGL, second-order, consistent mass matrix:

$$\kappa \sim \left\{ \xi \left( 1 + \frac{128}{99225} \xi^8 \right), \frac{1}{4} \sqrt{210 - 6\sqrt{805}}, \frac{1}{4} \sqrt{42}, \frac{1}{4} \sqrt{210 + 6\sqrt{805}} \right\},$$

$$S \sim \frac{2\xi^6}{5325075} \begin{pmatrix} 0 & -336\sqrt{805} & 0 & 336\sqrt{805} \\ 7360 & -16(230 + \sqrt{805}) & 0 & -16(230 - \sqrt{805}) \\ -11270 & 7(805 + 17\sqrt{805}) & 0 & 7(805 - 17\sqrt{805}) \\ 7360 & -16(230 + \sqrt{805}) & 0 & -16(230 - \sqrt{805}) \end{pmatrix}.$$

$M = 4$ , LGL, second-order, lumped mass matrix:

$$\kappa \sim \left\{ \xi \left( 1 - \frac{32}{99225} \xi^8 \right), \sqrt{\frac{1}{8}(55 - \sqrt{1345})}, \sqrt{21/8}, \sqrt{\frac{1}{8}(55 + \sqrt{1345})} \right\},$$

$$S \sim \frac{\xi^6}{20760075} \begin{pmatrix} 0 & 3136\sqrt{1345} & 0 & -3136\sqrt{1345} \\ -86080 & 32(1345 + 13\sqrt{1345}) & 0 & 32(1345 - 13\sqrt{1345}) \\ 131810 & -49(1345 + 31\sqrt{1345}) & 0 & -49(1345 - 31\sqrt{1345}) \\ -86080 & 32(1345 + 13\sqrt{1345}) & 0 & 32(1345 - 13\sqrt{1345}) \end{pmatrix}.$$

$M = 5$ , LGL, first-order, consistent mass matrix:

$$\kappa \sim \left\{ -\frac{2}{5}\sqrt{3(10+3\sqrt{5})}, -\frac{2}{5}\sqrt{3(10-3\sqrt{5})}, \xi\left(1 - \frac{9765625}{19179224064}\xi^{12}\right), \frac{2}{5}\sqrt{3(10-3\sqrt{5})}, \frac{2}{5}\sqrt{3(10+3\sqrt{5})} \right\},$$

$$S \sim \frac{3125\xi^6}{133056} \begin{pmatrix} -\frac{1}{36}(9+5\sqrt{5}) & -\frac{1}{36}(9-5\sqrt{5}) & 1 & -\frac{1}{36}(9-5\sqrt{5}) & -\frac{1}{36}(9+5\sqrt{5}) \\ 0.1118+0.2522i & 0.04879-0.04359i & -\frac{1}{63}(7+5\sqrt{7}) & 0.04879+0.04359i & 0.1118-0.2522i \\ -0.008881-0.1704i & -0.04055-0.04945i & -\frac{1}{63}(7-5\sqrt{7}) & -0.04055+0.04945i & -0.008881+0.1704i \\ -0.008881+0.1704i & -0.04055+0.04945i & -\frac{1}{63}(7-5\sqrt{7}) & -0.04055-0.04945i & -0.008881-0.1704i \\ 0.1118-0.2522i & 0.04879+0.04359i & -\frac{1}{63}(7+5\sqrt{7}) & 0.04879-0.04359i & 0.1118+0.2522i \end{pmatrix}.$$

The closed-form expressions for the numerical entries are a bit lengthy. Let  $S = s_{1,3}H$ . Then,

$$h_{2,1} = \frac{1}{756}(21 + 8\sqrt{5} + 15\sqrt{7} + \sqrt{35}) + \frac{i}{1764}\sqrt{77(980 + 399\sqrt{5} + 130\sqrt{7} + 60\sqrt{35})},$$

$$h_{2,2} = \frac{1}{756}(21 - 8\sqrt{5} + 15\sqrt{7} - \sqrt{35}) - \frac{i}{1764}\sqrt{77(980 - 399\sqrt{5} + 130\sqrt{7} - 60\sqrt{35})},$$

and

$$h_{k,5} = h_{k,1}^*, \quad h_{k,4} = h_{k,2}^*, \quad h_{5,k} = h_{2,k}^*, \quad h_{4,k} = h_{3,k}^*, \quad k = 1, \dots, 5.$$

$M = 5$ , LGL, first-order, lumped mass matrix:

$$\kappa \sim \left\{ -\frac{2}{5}\sqrt{3(7+\sqrt{14})}, -\frac{2}{5}\sqrt{3(7-\sqrt{14})}, \xi\left(1 - \frac{78125}{67060224}\xi^{10}\right), \frac{2}{5}\sqrt{3(7-\sqrt{14})}, \frac{2}{5}\sqrt{3(7+\sqrt{14})} \right\},$$

$$S \sim \frac{625\xi^6}{12096} \begin{pmatrix} -0.5618 & 0.0618 & 1 & 0.0618 & -0.5618 \\ 0.1025+0.2115i & 0.058-0.04849i & -0.3211 & 0.058+0.04849i & 0.1025-0.2115i \\ -0.002446-0.1207i & -0.04699-0.05795i & 0.09887 & -0.04699+0.05795i & -0.002446+0.1207i \\ -0.002446+0.1207i & -0.04699+0.05795i & 0.09887 & -0.04699-0.05795i & -0.002446-0.1207i \\ 0.1025-0.2115i & 0.058+0.04849i & -0.3211 & 0.058-0.04849i & 0.1025+0.2115i \end{pmatrix}.$$

Again, with  $S = s_{1,3}H$ , we have

$$h_{1,1} = -\frac{1}{12}(3 + \sqrt{14}), \quad h_{1,2} = -\frac{1}{12}(3 - \sqrt{14}),$$

$$h_{2,1} = \frac{1}{504}(14 + 10\sqrt{7} + 3\sqrt{14}) + \frac{i}{504}\sqrt{70(59 + 20\sqrt{2} + 10\sqrt{7} + 13\sqrt{14})},$$

$$h_{2,2} = \frac{1}{504}(14 + 10\sqrt{7} - 3\sqrt{14}) - \frac{i}{504}\sqrt{70(59 - 20\sqrt{2} + 10\sqrt{7} - 13\sqrt{14})},$$

$$h_{3,1} = \frac{1}{504}(14 - 10\sqrt{7} + 3\sqrt{14}) - \frac{i}{504}\sqrt{70(59 - 20\sqrt{2} - 10\sqrt{7} + 13\sqrt{14})},$$

$$h_{3,2} = \frac{1}{504}(14 - 10\sqrt{7} - 3\sqrt{14}) - \frac{i}{504}\sqrt{70(59 + 20\sqrt{2} - 10\sqrt{7} - 13\sqrt{14})},$$

$$h_{2,3} = -(7 + 5\sqrt{7})/63, \quad h_{3,3} = -(7 - 5\sqrt{7})/63,$$

and the other entries follow the same symmetry pattern as in the previous case.  $M = 5$ , LGL, second-order, consistent mass matrix:

$$\kappa \sim \left\{ \xi\left(1 + \frac{390625}{804722688}\xi^{10}\right), \frac{2}{5}\sqrt{3(10-3\sqrt{5})}, \frac{1}{5}\sqrt{6(35 - \sqrt{805})}, \frac{2}{5}\sqrt{3(10+3\sqrt{5})}, \frac{1}{5}\sqrt{6(35 + \sqrt{805})} \right\},$$

$$\begin{aligned}
S &\sim i \frac{15625\xi^7}{58677696} \begin{pmatrix} 0 & 0 & 0 & 0 \\ -\frac{2}{3}\sqrt{3(49-10\sqrt{7})} & -\sqrt{\frac{1}{21}(763-210\sqrt{5}-2\sqrt{35(761-336\sqrt{5})})} & 0 & \sqrt{\frac{1}{21}(763+210\sqrt{5}+2\sqrt{35(761-336\sqrt{5})})} \\ \frac{2}{3}\sqrt{3(49+10\sqrt{7})} & -\sqrt{\frac{1}{21}(763-210\sqrt{5}+2\sqrt{35(761-336\sqrt{5})})} & 0 & -\sqrt{\frac{1}{21}(763+210\sqrt{5}-2\sqrt{35(761-336\sqrt{5})})} \\ -\frac{2}{3}\sqrt{3(49+10\sqrt{7})} & \sqrt{\frac{1}{21}(763-210\sqrt{5}+2\sqrt{35(761-336\sqrt{5})})} & 0 & \sqrt{\frac{1}{21}(763+210\sqrt{5}-2\sqrt{35(761-336\sqrt{5})})} \\ \frac{2}{3}\sqrt{3(49-10\sqrt{7})} & \sqrt{\frac{1}{21}(763-210\sqrt{5}-2\sqrt{35(761-336\sqrt{5})})} & 0 & -\sqrt{\frac{1}{21}(763+210\sqrt{5}+2\sqrt{35(761-336\sqrt{5})})} \end{pmatrix} \\
&\sim i \frac{15625\xi^7}{58677696} \begin{pmatrix} 0 & 0 & 0 & 0 & 0 \\ -5.48 & -3.50 & 0 & 8.98 & 0 \\ 10.03 & -3.97 & 0 & -6.06 & 0 \\ -10.03 & 3.97 & 0 & 6.06 & 0 \\ 5.48 & 3.50 & 0 & -8.98 & 0 \end{pmatrix}.
\end{aligned}$$

$M = 5$ , LGL, second-order, lumped mass matrix:

$$\begin{aligned}
\kappa &\sim \left\{ \xi \left( 1 - \frac{78125}{804722688} \xi^{10} \right), \frac{2}{5} \sqrt{3(7-\sqrt{14})}, \frac{1}{5} \sqrt{6(35-\sqrt{805})}, \frac{2}{5} \sqrt{3(7+\sqrt{14})}, \frac{1}{5} \sqrt{6(35+\sqrt{805})} \right\}, \\
S &\sim i \frac{3125\xi^7}{32006016} \begin{pmatrix} 0 & 0 & 0 & 0 \\ 2\sqrt{3(49-10\sqrt{7})} & \sqrt{\frac{3}{2}(231-32\sqrt{14}-10\sqrt{7(23-6\sqrt{14})})} & 0 & -\sqrt{\frac{3}{2}(231+32\sqrt{14}+10\sqrt{7(23+6\sqrt{14})})} \\ -2\sqrt{3(49+10\sqrt{7})} & \sqrt{\frac{3}{2}(231-32\sqrt{14}+10\sqrt{7(23-6\sqrt{14})})} & 0 & \sqrt{\frac{3}{2}(231+32\sqrt{14}-10\sqrt{7(23+6\sqrt{14})})} \\ 2\sqrt{3(49+10\sqrt{7})} & -\sqrt{\frac{3}{2}(231-32\sqrt{14}+10\sqrt{7(23-6\sqrt{14})})} & 0 & -\sqrt{\frac{3}{2}(231+32\sqrt{14}-10\sqrt{7(23+6\sqrt{14})})} \\ -2\sqrt{3(49-10\sqrt{7})} & -\sqrt{\frac{3}{2}(231-32\sqrt{14}-10\sqrt{7(23-6\sqrt{14})})} & 0 & \sqrt{\frac{3}{2}(231+32\sqrt{14}+10\sqrt{7(23+6\sqrt{14})})} \end{pmatrix} \\
&\sim i \frac{3125\xi^7}{32006016} \begin{pmatrix} 0 & 0 & 0 & 0 & 0 \\ 16.45 & 11.72 & 0 & -28.17 & 0 \\ -30.09 & 14.01 & 0 & 16.08 & 0 \\ 30.09 & -14.01 & 0 & -16.08 & 0 \\ -16.45 & -11.72 & 0 & 28.17 & 0 \end{pmatrix}.
\end{aligned}$$

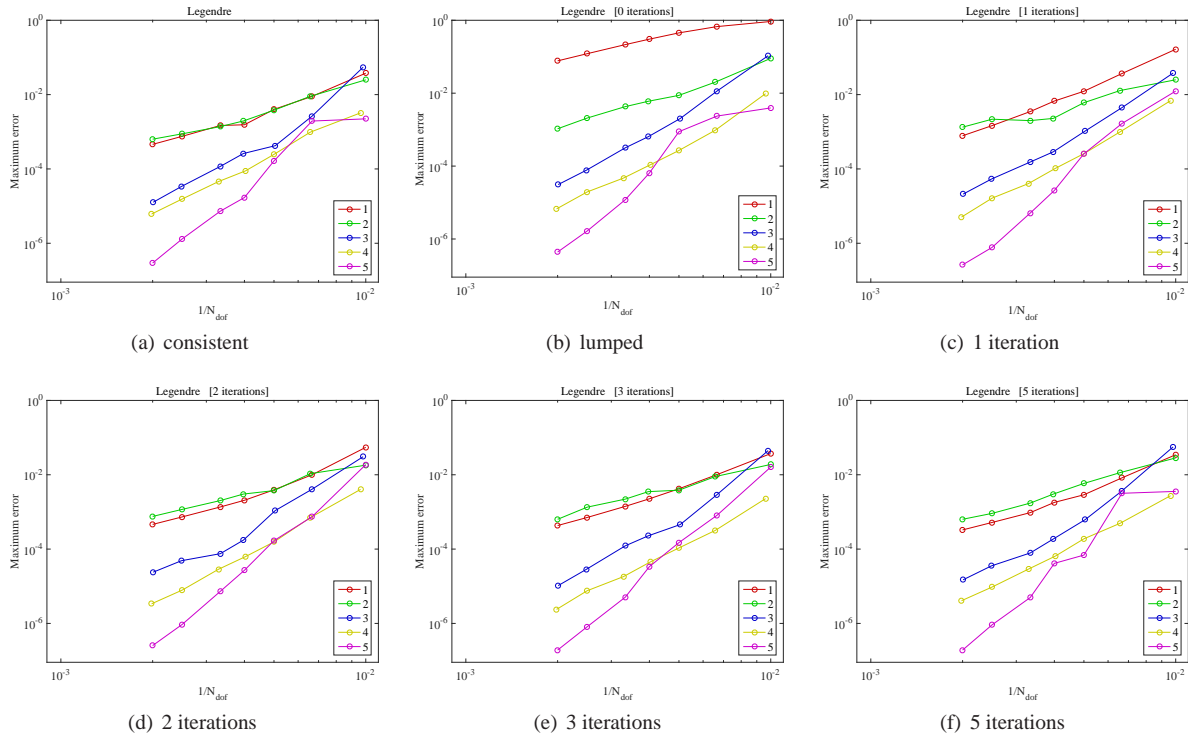


Figure 5: Maximum error in the particle velocity,  $v$ , as function of the inverse number of degree of freedom,  $1/N_{\text{dof}}$ , for the Legendre-Gauss-Lobatto nodes (LGL) with (a) the consistent mass matrix, (b) the lumped mass matrix, and after 1 (c), 2 (d), 3 (e) or 5 (f) iterations with the defect correction operator  $\mathcal{G}$ .

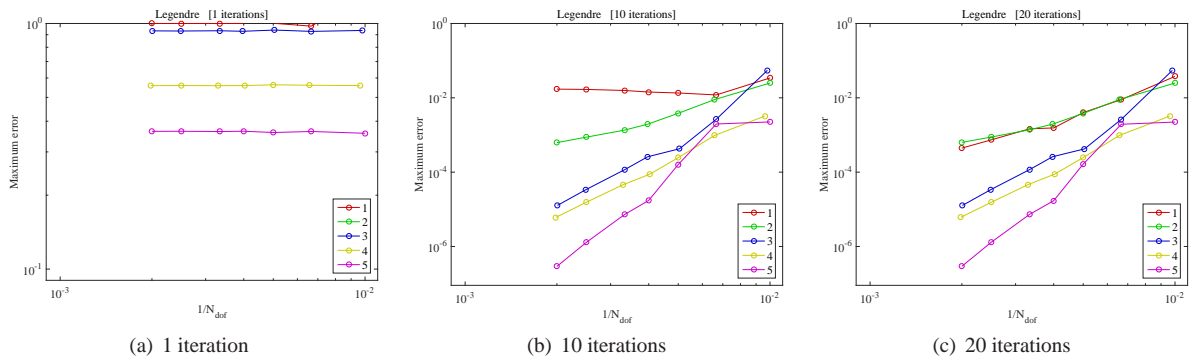


Figure 6: Maximum error in the particle velocity,  $v$ , as function of the inverse number of degree of freedom,  $1/N_{\text{dof}}$ , for the Legendre-Gauss-Lobatto nodes (LGL) using the diagonal of the mass matrix as preconditioner, after 1 (a), 10 (b), or 20 (c) iterations.

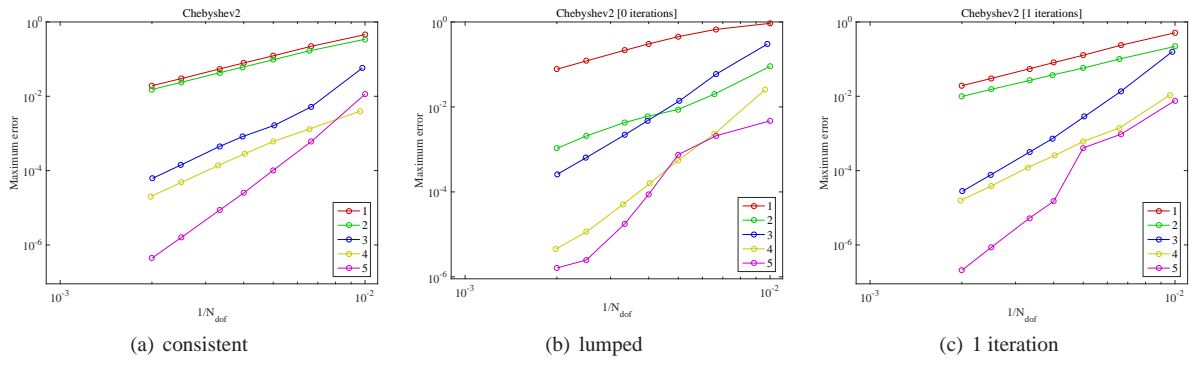


Figure 7: Maximum error in the particle velocity,  $v$ , as function of the inverse number of degree of freedom,  $1/N_{\text{dof}}$ , for the Chebyshev-Gauss-Lobatto nodes with weighting (CGLw) with the consistent mass matrix (a), its lumped version (b), or with one iteration (c).